Cationic membranes complexed with oppositely charged microtubules: hierarchical self-assembly leading to bio-nanotubes

2006 J. Phys.: Condens. Matter 18 S1271

(http://iopscience.iop.org/0953-8984/18/28/S10)

INSTITUTE OF PHYSICS PUBLISHING JOURNAL OF PHYSICS: CONDENSED MATTER

J. Phys.: Condens. Matter **18** (2006) S1271–S1279 doi:10.1088/0953-8984/18/28/S10

Cationic membranes complexed with oppositely charged microtubules: hierarchical self-assembly leading to bio-nanotubes

Uri Raviv[1,2,3,4,5], **Daniel J Needleman**[1,2,3,6] **and Cyrus R Safinya**[1,2,3,5]

[1] Materials Department, University of California, Santa Barbara, CA 93106, USA
[2] Physics Department, University of California, Santa Barbara, CA 93106, USA
[3] Molecular, Cellular, and Developmental Biology Department, University of California, Santa Barbara, CA 93106, USA

E-mail: raviv@chem.ch.huji.edu and safinya@mrl.ucsb.edu

Received 13 March 2006, in final form 16 May 2006
Published 28 June 2006
Online at stacks.iop.org/JPhysCM/18/S1271

Abstract

The self-assembly of microtubules and charged membranes has been studied, using x-ray diffraction and electron microscopy. Polyelectrolyte lipid complexes usually form structures templated by the lipid phase, when the polyelectrolyte curvature is much larger than the membrane spontaneous curvature. When the polyelectrolyte curvature approaches the membrane spontaneous curvature, as in microtubules, two types of new structures emerge. Depending on the conditions, vesicles either adsorb onto the microtubule, forming a 'beads on a rod' structure, or coat the microtubule, which now forms the template. Tubulin oligomers then coat the external lipid layer, forming a lipid protein nanotube. The tubulin oligomer coverage at the external layer is determined by the membrane charge density. The energy barrier between the beads on a rod and the lipid–protein nanotube states depends on the membrane bending rigidity and membrane charge density. By controlling the lipid/tubulin stoichiometry we can switch between lipid–protein nanotubes with open ends to lipid–protein nanotubes with closed end with lipid cups. This forms the basis for controlled drug encapsulation and release.

(Some figures in this article are in colour only in the electronic version)

1. Introduction

We are investigating the assemblies of charged biopolymers and oppositely charged membranes. More specifically we would like to understand what the threshold conditions

[4] Present address: The Department of Physical Chemistry, The Institute of Chemistry, The Hebrew University of Jerusalem, Givat Ram, 91904, Jerusalem, Israel.
[5] Authors to whom any correspondence should be addressed.
[6] Present address: Harvard Medical School, Harvard University, Boston, MA, USA.

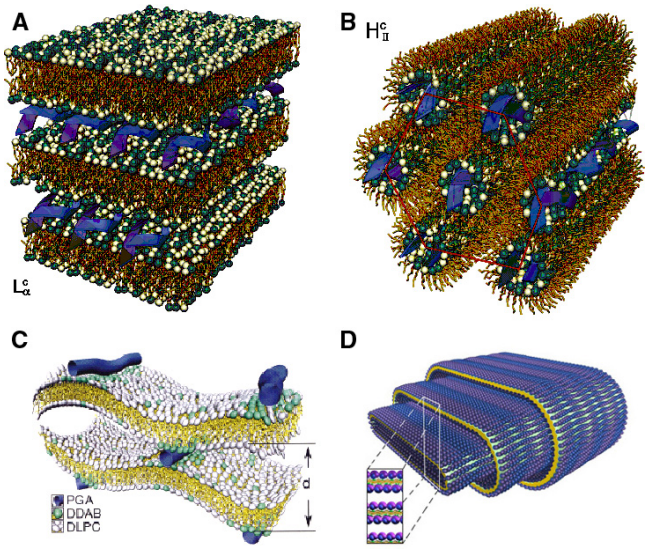

Sketch 1. (A) Cationic lipid–DNA complexes in the multilamellar phase with flat membranes [5]. (B) Cationic lipid–DNA complexes in the inverted hexagonal phase [3]. (C) Cationic lipid–poly(glutamic acid) complexes showing pinched membranes [8]. (D) Cationic lipid–F-Actin complexes showing swollen membranes [9].

are for a charged membrane to encapsulate an oppositely charged biopolymer, as occurs in nonspecific endocytosis, and when there is only adsorption of the biopolymer on the membrane [1]. Complexes of lipids and oppositely charged proteins or biopolymers have applications in drug and gene delivery [2–5] and they form a class of interesting biomaterials [6].

When mixing cationic lipids and DNA, DNA–lipid complexes are formed and used to deliver genes into cells [2–4]. The complexes can be in the lamellar phase, composed of alternating DNA monolayers and lipid bilayers (sketch 1(A)). When the spontaneous curvature of the lipids is negative a transition to inverted hexagonal phase occurs, at which the DNA molecules are coated by a lipid monolayer and arranged in a hexagonal array (sketch 1(B)). The inverted hexagonal phase has a higher transfection efficiency [3]. This demonstrates that the structure of lipid–biopolyelectrolyte complexes may profoundly affect their function.

The formation of the complexes is due to an entropy gain. We start with charged rods that have counterions that condense until the effective linear charge density is one electron per Bjerrum length, which is about 7 Å in water. The membranes are also charged and most of their counterions are confined to a very thin layer. When we mix the charged rods and the oppositely charged membranes, they can neutralize each other and most of their counterions can be released into solution, where they gain solution entropy [7].

Polyelectrolyte lipid complexes (PLCs) that have been studied so far adopt mainly the multilamellar phase, which is templated by the original lipid symmetry; however, different PLCs still exhibit various morphologies. Pinched multilamellar PLCs (sketch 1(C)) are obtained when poly(glutamic acid) (PGA), which is a negatively charged polypeptide with a charge density of about 6 e nm^{-3}, a diameter of 1 nm and a persistence length of 2 nm, is complexed with cationic membranes [8]. Flat (thermally fluctuating) multilamellar PLCs (sketch 1(A)) are obtained when lambda DNA, which has a negative charge density of about 2 e nm^{-3}, a diameter of 2 nm and a persistence length of 50 nm, is complexed with cationic

membranes [5]. Swollen multilamellar PLCs (sketch 1(D)), at which each lipid bilayer is coated from either sides by an oppositely charged hydrated polyelectrolyte monolayer, are obtained when filamentous actin (F-actin), which has a negative surface charge density of 0.3 e nm^{-3}, a diameter of 8 nm and a persistence length of 10 μm, is complexed with cationic membranes [9]. Moreover, within the polyelectrolyte layers that form on the cationic lipid membranes, the degree of order increases with increasing polymer diameter and rigidity. For PGA we get no order; DNA forms 1D crystals on the membranes, such that the spacing between the DNA rods is well defined; however, the DNA rods can still slide with respect to each other. F-actin molecules are even more ordered and form 2D crystals on the cationic membranes. The common feature for all of these structures is that they are templated by the original multilamellar phase of the lipid bilayers and the biopolymers just adsorb on the membranes and are incorporated between the membranes.

Microtubules (MTs) are net negatively charged polymers, which self-assemble from tubulin protein subunits into hollow cylinders. The tubulin dimers are arranged head to tail in protofilaments and form the MT wall. MTs are critical components in a broad range of functions in eukaryotic cells—from providing tracks for the transport of cargo to forming the spindle structure for chromosome segregation before cell division. They are used as nanometre-scale tracks in neurons for the transport of neurotransmitter precursors and enzymes to synaptic junctions in nerve cell communication.

An MT has a charge density of 0.2 e nm^{-3}, an outer diameter of about 26 nm, inner diameter of about 16 nm and a persistence length of several millimetres, and represents an extreme case of polymer outer diameter and rigidity. It was therefore of interest to study the structures and interactions between MTs and cationic lipid bilayers. Unlike most of the other complexes at which the membrane bending energy overcomes the electrostatic interactions, here the reverse is true. We found that the MTs formed the template for the complex structure.

Using synchrotron small angle x-ray diffraction (SAXRD) and transmission electron microscopy (TEM), we find two novel structures [10]. For soft and intermediate rigid membranes we find that the cationic liposomes spread and coat the MTs and the external lipid layer is decorated by tubulin oligomers, forming a novel lipid–protein nanotube (LPN). By controlling the cationic lipid/tubulin stoichiometry, $R_{CL/T}$, of the complex the LPN can switch between a state with open ends (sketch 2(A)) to a state with closed ends with lipid caps (sketch 2(B)). This forms the basis for controlled drug encapsulation and release.

For low membrane charge density, we find that vesicles adsorb onto the MT and appear as 'beads on a rod' (BOR) (sketch 2(C)). This is the most trivial structure that can form when vesicles interact with polyelectrolytes and was previously hypothesized for cationic lipid–DNA complexes [11], but later was experimentally [3, 5] proven unstable. Here we discovered for the first time how to obtain BOR. This state, however, seems to be a kinetically trapped state. The ground state of the system follows the MT template and forms the LPN.

2. Experimental details

Tubulin was purified from bovine brains and was polymerized and taxol stabilized as described elsewhere [10, 12]. The cationic lipid used was dioleoyl($C_{18:1}$)–trimethyl ammonium propane (DOTAP). The membrane charge density, σ, was adjusted by adding a homologous neutral lipid with the same hydrophobic tail to the charged lipid, but with the phosphatidylcholine (PC) head group instead (DOPC). Equal volumes of MTs and liposome solutions were mixed and the resulting complexes were characterized by transmission electron microscopy (TEM) and small angle x-ray diffraction (SAXRD) performed at Stanford Synchrotron Radiation Laboratory, beam-line 4-2.

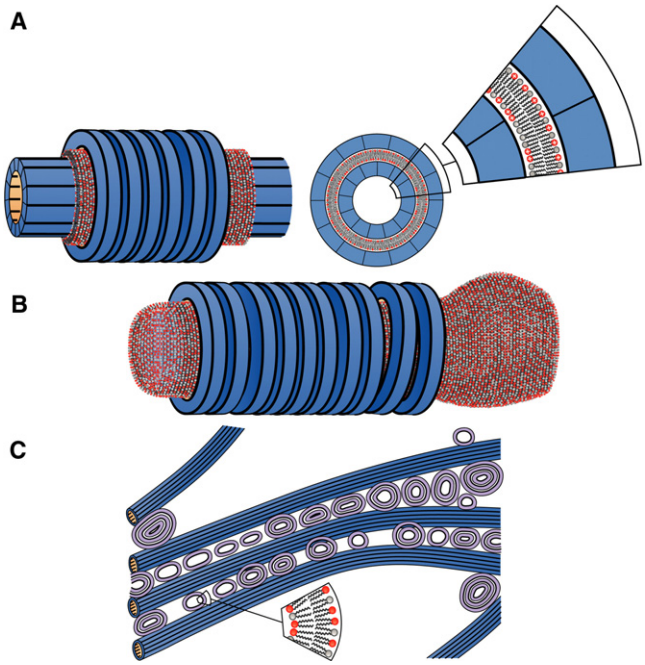

Sketch 2. (A) Lipid–protein nanotube (LPN) with open ends and a cross section. (B) LPN with closed end and lipid caps. (C) Beads on rod structure.

The mole fraction of cationic lipids in the membrane is given by

$$x_{\mathrm{CL}} \equiv N_{\mathrm{CL}}/(N_{\mathrm{CL}} + N_{\mathrm{NL}}),$$

where N_{CL} and N_{NL} are the numbers of cationic and neutral lipids, respectively. The relative cationic lipid/tubulin stoichiometry, $R_{\mathrm{CL/T}}$, is defined as

$$R_{\mathrm{CL/T}} \equiv N_{\mathrm{CL}}/N_{\mathrm{T}},$$

where N_{T} is the number of tubulin dimers. $R_{\mathrm{CL/T}} \approx 40$ is the mixing isoelectric point.

3. Results and discussion

A set of TEM images covering the structures in the phase diagram of MT–membrane complexes is shown in figure 1. For cationic lipid mole fraction, $x_{\mathrm{CL}} = 0.1$, we initially find the weakly positive charged vesicles ('beads') adsorbed onto the negatively charged microtubule, MT, wall ('rod'), forming the beads on a rod, BOR (figure 1(A)). Bridges are occasionally formed between adjacent MTs forming small sized bundles of MTs cross-linked via vesicles (figure 1(B)). This state is, however, kinetically trapped: over longer times, ∼60 h, the adsorbed vesicles 'wet' the MT surface, forming the lipid–protein nanotube, LPN (figure 1(C)). For $x_{\mathrm{CL}} > 0.1$ the LPN forms immediately upon mixing. The images reveal that the LPN is made of three layers: intact MTs are coated by a lipid bilayer (appears brighter in the images, as the ionic stain avoids the hydrophobic lipid tails), which in turn are coated by tubulin oligomers forming rings or spirals. The oligomer orientation is perpendicular to the internal MT protofilament direction and their density increases with x_{CL}. The three layered LPN structure

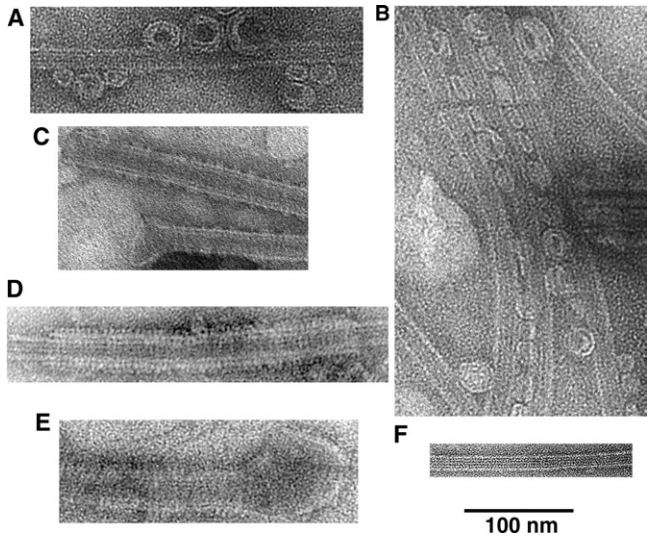

Figure 1. *Transmission electron microscopy images of the various states.* Whole mount images of liposome–MT complexes, using DOTAP/DOPC solutions with $x_{CL} \equiv N_{CL}/(N_{CL} + N_{NL})$ and $R_{CL/T} \equiv N_{CL}/N_T$ values as follows. (A)–(C) $x_{CL} = 0.1$, $R_{CL/T} = 16$ showing the beads on a rod phase (A) and the bridging phase (B), which are kinetically trapped states. The lipid protein nanotube (LPN) state (C) is obtained after time $\Delta t \sim 60$ h. (D) and E correspond to LPN with open ends (D) and closed ends (E) obtained with $x_{CL} = 0.5$ and $R_{CL/T} = 40$ (in D) and $R_{CL/T} = 120$ (in E). As a control a pure MT is shown in (F).

arises because of the mismatch between the charge densities of MTs and cationic membranes. The oligomers coat the external lipid monolayer to optimize the electrostatic interactions and counterion release.

At a given mole fraction of cationic lipids, x_{CL}, when the total MT surface area exceeds the total membrane area, the MTs are only partially coated (figure 1(D), $x_{CL} = 0.5$ and cationic lipid/tubulin stoichiometry, $R_{CL/T} = 40$), forming LPNs with open ends. When the reverse is true, some of the excess vesicles are attached primarily to the ends of the LPNs (figure 1(E), $x_{CL} = 0.5$, $R_{CL/T} = 120$), forming LPNs with closed ends with lipid caps. The oligomer density at a given x_{CL} is similar for both open and closed LPNs. The ability to switch from open to closed LPNs forms the basis of controlled drug encapsulation and release.

TEM images and SAXRD measurements performed on pure microtubule, MT, solutions (figures 1(F) and 2) and are in agreement with earlier studies [12–16]. The SAXRD profile of MTs (figure 2(A)) is consistent with the form factor of isotropic hollow cylinders (figure 2(B)). Based on MT structural data [13, 17], we modelled the MT as three concentric cylindrical shells, of a high electron density region surrounded by two low ones, as shown in figure 2(C), keeping the total wall thickness and mean electron density as those of MTs. The thickness and location of the high electron density region, within the MT wall, and the inner MT radius are fitting parameters in this model.

A set of SAXRD data for MT–lipid (DOTAP/DOPC) complexes is shown in figure 2(A). For $x_{CL} > 0.1$ the SAXRD scans show broad oscillations that are different from that of MTs and correspond to the form factor of the LPNs. For $x_{CL} = 0.1$, 2 h after MTs and membranes were mixed, the SAXRD scan is consistent (for $q > 0.2\ \text{nm}^{-1}$) with the form factor of isotropic MT solutions. At smaller angles there is an additional broad Gaussian correlation peak, centred at $q = 0.139\ \text{nm}^{-1}$, corresponding to 45 nm. The SAXRD scan is therefore consistent with the

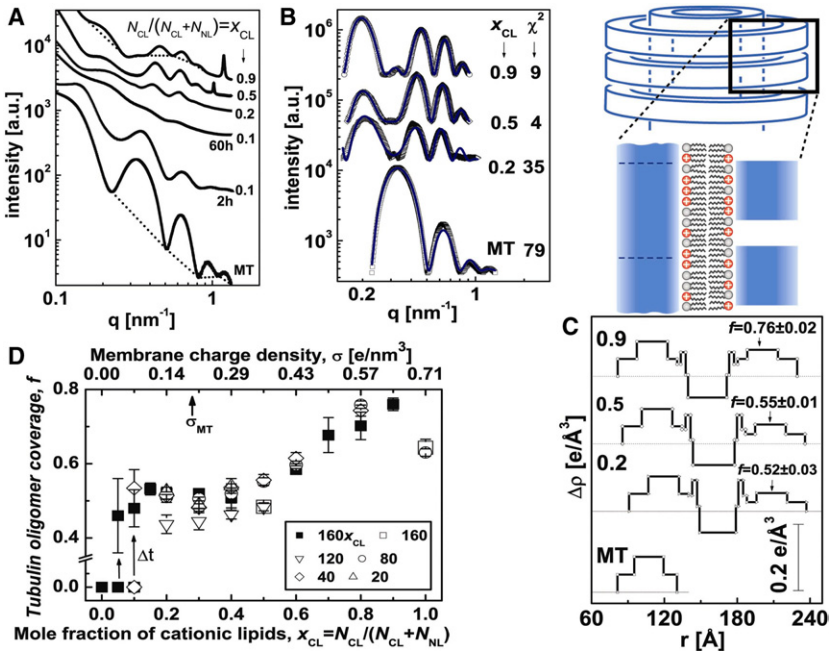

Figure 2. *Synchrotron small angle x-ray scattering data, analysis and a state diagram.* (A) Radially averaged scattering intensities of MTs and MT–lipid complexes (solid symbols), using DOTAP/DOPC solutions with $x_{CL} \equiv N_{CL}/(N_{CL} + N_{NL})$ as indicated in the figure. $R_{CL/T} \equiv N_{CL}/N_T$ is given by $R_{CL/T} = 160{\cdot}x_{CL}$, corresponding to the point at which the total amount of lipid is exactly enough to coat each MT with a bilayer. For $x_{CL} = 0.1$ two scans are shown, 2 and 60 h after preparing the sample. The broken curves are examples of the assumed background [12, 14, 15]. (B) Scattering data from (A), following background subtraction (open symbols). The solid curves are the fitted scattering models. Their χ^2 values are as in the figure. (C) The variation of the radial electron density, $\Delta\rho(r)$, relative to water (broken lines), of the MTs and complex walls, obtained from fitting the scattering data in (B) to models of concentric cylinders. r is the distance from the centre of the cylinders. The tubulin oligomer coverage, f, values obtained from the nonlinear fit are indicated on the right-hand side. The schematic diagram represents a vertical cut through the MT–membrane–tubulin complex wall, corresponding to $\Delta\rho(r)$. (D) A state diagram: f as a function of x_{CL} or the membrane charge density, σ, when lipids can fully cover the MTs. Each data point is based on scattering data and models as in (A)–(C). Solid squares corresponds to $R_{CL/T} = 160 \cdot x_{CL}$. Open symbols represent different $R_{CL/T}$ values, as indicated in the figure. For $0 < x_{CL} \leqslant 0.1$ we initially get $f = 0$ (corresponding to the BOR structure); over time, $\Delta t \sim 60$ h, shown by the arrows, we obtain LPNs with higher f values.

BOR and bridging states (figure 1). The existence of a correlation peak suggests that the size distribution of the bridging vesicles is relatively narrow. SAXRD scans taken 60 h after mixing (figure 2(A)) show that this structure slowly evolves into the form factor of the LPNs.

To gain quantitative insight into the organization of the complexes, we analyse the background subtracted SAXRD data, shown in figure 2(B), by fitting to a model. To model the data, a series of power laws that pass through the minima of the scattering intensities was subtracted. We extend the isotropic concentric cylindrical shells model of MTs to include the second lipid bilayer and the third tubulin layer (figure 2(C)). The radial electron density profile of the inner MT wall and outer tubulin monolayer are based on the fit to the MT scattering data. The parameters for the electron density profile of the lipid bilayer are based on literature data [9, 18]. Finally, the third tubulin layer is multiplied by the fraction, f, of tubulin coverage

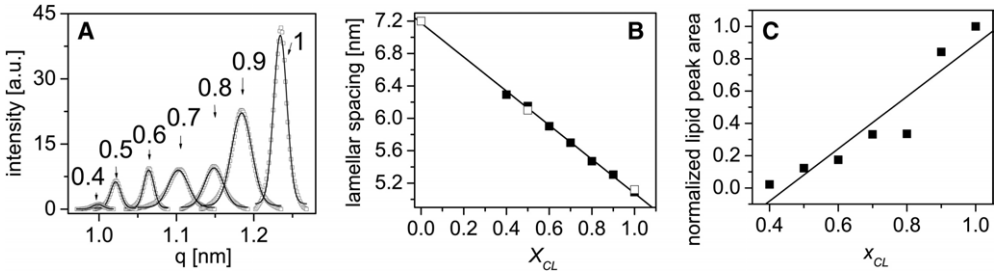

Figure 3. Excess lipid peaks. (A) Radially averaged and background subtracted scattering intensities of MT–lipid complexes, at $0.9 \leqslant q \leqslant 1.3$ nm^{-1}, using DOTAP/DOPC solutions with cationic lipid mole fraction, x_{CL}, values as indicated in the figure. The membrane/tubulin stoichiometry $R_{\mathrm{CL/T}}$ is given by $R_{\mathrm{CL/T}} = 160x_{\mathrm{CL}}$ (as in figure 2(A)). The solid curves are fits to Gaussians. (B) From the Gaussian peak centre we determined the periodicity of the lipid bilayer multilamellar phase. The lamellar spacing is plotted as a function of x_{CL}. Solid symbols are for the excess lipid peaks of the MT–lipid complexes. Open symbols are for pure DOTAP/DOPC lipid mixtures in the same PEM buffer solution, falling exactly on the same curve as the excess lipid peaks. (C) The normalized area under the Gaussian excess lipid peaks as a function of x_{CL}, assuming the peak at $x_{\mathrm{CL}} = 1$ has an area of 1.

relative to the inner MT wall. f is the unknown parameter in this model and is allowed to float freely. The scattering models (figure 2(B)) fit very well to the data.

Figure 2(D) summarizes a series of SAXRD scans as in figure 2(A), analysed as in figures 2(B) and (C). A state diagram is obtained, in which f is plotted as a function of x_{CL} or the membrane charge density, σ, at various $R_{\mathrm{CL/T}}$ values. For $x_{\mathrm{CL}} = 0$, corresponding to the pure DOPC membrane, SAXRD scans show only the isotropic MT form factor. This state (indicated as $f = 0$) is stable for days, indicating that the LPN is induced by the cationic lipids. At $0 < x_{\mathrm{CL}} \leqslant 0.1$, we have kinetically trapped states of BOR and bridging (also indicated by $f = 0$) that evolve slowly into the LPN. For $x_{\mathrm{CL}} > 0.1$, we only see the LPN with f values that increase monotonically with x_{CL}. $R_{\mathrm{CL/T}}$ has little effect on f, in agreement with the TEM images (figure 1).

The SAXRD scans may also have a resolution limited strong peak (figure 2(A) $x_{\mathrm{CL}} = 0.5$, 0.9), corresponding to the (001) peak of a one-dimensional lamellar structure. In figure 3(A) we plot the peaks obtained at different x_{CL} values and we fit them to Gaussians. In figure 3(B) we plot the lamellar spacing obtained from the fit as a function of x_{CL}. Independent control measurements (figure 3(B), open symbols) on pure DOTAP/DOPC lipid mixtures in the same PEM buffer solution showed exactly the same peak. The peak was therefore attributed to excess lipid vesicles in the lamellar phase with composition similar to the original membranes. TEM images (see figure 1(E)) show that, when an excess lipid peak can be detected, excess vesicles are attached to the ends of the tubular complex, forming a LPN with closed ends. The vesicles go to the ends of the tubular complexes to allow their counterions to travel about the volume of the whole complex, rather than to be confined to the vicinity of the membrane sheets. By doing so, the counterions gain entropy. The vesicles at the ends of the LPN may also reduce edge effects.

The intensity of the excess lipid peak is controlled by the membrane/tubulin stoichiometry (figure 4). We did not observe the excess lipid peak below $x_{\mathrm{CL}} = 0.3$, even when the total surface area of the lipids was much more than needed to cover all the MTs. As shown in figure 3(C), when the total amount of lipids was kept constant, above $x_{\mathrm{CL}} = 0.3$, the area under the excess lipid peak was increasing with x_{CL}. This suggests that membranes with larger x_{CL} have greater propensity to associate with the LPNs. The excess vesicles that associate with

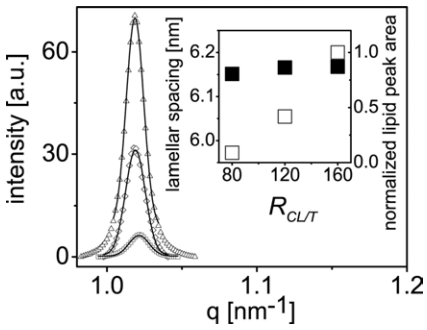

Figure 4. Excess lipid peaks following background subtraction, using DOTAP/DOPC solutions with $x_{CL} = 0.5$, at different membrane/tubulin stoichiometry ratios, $R_{CL/T}$. Squares indicate $R_{CL/T} = 80$, diamonds indicate $R_{CL/T} = 120$ and triangles indicate $R_{CL/T} = 160$. The solid curves are fits to Gaussians. Inset: the lamellar spacing and the normalized area under the Gaussian peaks as a function of $R_{CL/T}$, assuming the peak at $R_{CL/T} = 160$ has an area of 1. Open square symbols indicate the normalized area under the peaks and the solid square symbols indicate the lamellar spacing.

the complexes still have nearly the same amount of neutral lipids as in the original membrane because they show the same lamellar spacing (figure 3(B)). In this way the lipid mixing entropy is maximized. The mean lamellar spacing decreased linearly with x_{CL} (figure 3(B)). This is because there are fewer DOPC molecules with increasing x_{CL}. The buffer contains about 70 mM monovalent salt and thus the electrostatic interactions are well screened. The hydrated phosphate head group of the neutral lipid (DOPC) is about 1 nm, so as we have less of it, the mean lamellar spacing decreases. When two DOPC membranes are facing each other we expect the lamellar spacing to increase by about 2 nm compared to DOTAP membranes, as observed. We further checked that at a given x_{CL}, increasing the membrane/tubulin stoichiometric ratio beyond the isoelectric point does not change the position of the excess lipid peak, but increases its intensity (figure 4). The area below the excess lipid peak increases linearly with $R_{CL/T}$, supporting the hypothesis that the excess lipid peak is mainly due to excess cationic lipids associated with the LPNs.

By changing the lipid hydrophobic tail the membrane bending rigidity, κ, was varied. When DLTAP/DLPC lipid solutions were used, κ was lower than with DOTAP/DOPC, whereas for DPTAP/DPPC solutions the lipids were in their ordered gel phase at ambient room temperature and κ was much higher. We found [10] that with DLTAP/DLPC the kinetically trapped states were not observed, and only the LPN was observed, even at low membrane charge densities. The tubulin coverage at the third layer was within the range of those obtained with DOTAP/DOPC solutions. In contrast DPTAP/DPPC solutions show only the beads on rod (BOR) structure for all membrane charge densities. The BOR structure is stable for days and the transition to the LPN was not observed. It shows that κ along with the membrane charge density are setting the energy barrier between the BOR structure and the LPN.

To understand the observations we need to consider the interplay between the electrostatic and membrane elastic interactions in the complexes [1]. Pure electrostatic interactions favour the LPN structure, as the distance between the charged membrane and the polyelectrolyte is minimized and counterion release is optimized. The entropy gain from releasing the partially bound membrane and polyelectrolyte counterions from the diffuse screening layers into the bulk solution is $k_B T$ per ion. But this has to be balanced by the bending energy cost. A membrane of curvature C has elastic energy, F_{el}, that is given by $F_{elas}/A = 0.5\kappa(C - C_0)^2$,

where A is the membrane area. The coated LPN state is expected when the entropy gain exceeds the elastic energy cost.

We have described and characterized the beads on a rod and the lipid–protein nanotube, LPN, structures, the conditions for their formation and the transition between them. By controlling the cationic lipid /tubulin stoichiometry the LPN can be tailored to have open or closed ends with lipid caps. Because the main governing concepts for this self-assembly are general [1, 19], we expect synthetic analogues to follow similar assembly pathways, so that synthetic versions mimicking the LPNs (e.g. replacing microtubules with rigid polyelectrolytes) may have applications in chemical encapsulation and delivery. Finally, positively charged membranes are commonly used for non-viral drug and gene delivery and are introduced into cells [3]. Our results suggest that their association with microtubules, leading to possible changes in their structure and dynamics in cells, is an important consideration in delivery applications using cationic lipids.

Acknowledgments

The work was performed using synchrotron x-ray scattering techniques at the Stanford Synchrotron Radiation Laboratory (SSRL) at beam-line 4-2, combined with sophisticated electron microscopy at the University of California, Santa Barbara. This project is supported by NSF DMR-0503347, CTS-0404444, and NIH GM-59288 and NS-13560. The Stanford Synchrotron Radiation Laboratory is supported by the US DOE. UR acknowledges the support of the International Human Frontier Science Program Organization and the European Molecular Biology Organization.

References

[1] Harries D, Ben-Shaul A and Szleifer I 2004 *J. Phys. Chem.* B **108** 1491–6
[2] Ewert K, Ahmad A, Evans H M, Schmidt H W and Safinya C R 2002 *J. Med. Chem.* **45** 5023–9
[3] Koltover I, Salditt T, Radler J O and Safinya C R 1998 *Science* **281** 78–81
[4] Safinya C R 2001 *Curr. Opin. Struct. Biol.* **11** 440–8
[5] Radler J O, Koltover I, Salditt T and Safinya C R 1997 *Science* **275** 810–4
[6] Koltover I, Sahu S and Davis N 2004 *Angew. Chem. Int. Edn* **43** 4034–7
[7] Bruinsma R 1998 *Eur. Phys. J.* B **4** 75–88
[8] Subramanian G, Hjelm R P, Deming T J, Smith G S, Li Y and Safinya C R 2000 *J. Am. Chem. Soc.* **122** 26–34
[9] Wong G C L, Tang J X, Lin A, Li Y, Janmey P A and Safinya C R 2000 *Science* **288** 2035–9
[10] Raviv U, Needleman D J, Li Y, Miller H P, Wilson L and Safinya C R 2005 *Proc. Natl Acad. Sci. USA* **102** 11167–72
[11] Felgner P L, Gadek T R, Holm M, Roman R, Chan H W, Wenz M, Northrop J P, Ringold G M and Danielsen M 1987 *Proc. Natl Acad. Sci. USA* **84** 7413–7
[12] Needleman D J, Ojeda-Lopez M A, Raviv U, Miller H P, Wilson L and Safinya C R 2004 *Proc. Natl Acad. Sci. USA* **101** 16099–103
[13] Li H, DeRosier D J, Nickolson W V, Nogales E and Downing K H 2002 *Structure* **10** 1317–28
[14] Andreu J M, Bordas J, Diaz J F, Garcia de Ancos J, Gil R, Medrano F J, Nogales E, Pantos E and Towns-Andrews E 1992 *J. Mol. Biol.* **226** 169–84
[15] Fernando-Diaz J, Andreu J M, Diakun G, Towns-Andrews E and Bordas J 1996 *Biophys. J.* **70** 2408–20
[16] Needleman D J, Ojeda-Lopez M A, Raviv U, Ewert K, Jones J B, Miller H P, Wilson L and Safinya C R 2004 *Phys. Rev. Lett.* **93** 198104
[17] Lee J C, Frigon R P and Timasheff S N 1973 *J. Biol. Chem.* **248** 7253–62
[18] Liu Y F and Nagle J F 2004 *Phys. Rev.* E **69** 040901
[19] May S and Ben-Shaul A 1997 *Biophys. J.* **73** 2427–40